

Detecting Ionospheric Gradients for GBAS Using a Null Space Monitor

Jing Jing, Samer Khanafseh, Fang-Cheng Chan, Steven Langel, Boris Pervan
Illinois Institute of Technology

Abstract—In this paper, a carrier phase-based monitor is developed to instantaneously detect ionospheric gradients using measurements from multiple, spatially separated ground antennas. Two monitor approaches based on traditional detection and estimation techniques are initially explored, and it is shown that their performance is highly dependent on how receivers' pairs (baselines) are selected for measurement differencing within a given spatial configuration. In order to eliminate this baseline selection dependency, a new monitor (termed the *null space monitor*) is proposed that combines measurements from a given set of spatially separated antennas through a null space transformation. In addition to the baseline selection independence, we show that the null space monitor has a larger gradient detection range than either of the two traditional monitors.

Keywords—Ionospheric gradient; GBAS; Null space

I. INTRODUCTION

Ground Based Augmentation Systems (GBAS) are safety-critical navigation systems intended to support all phases of approach, landing, departure, and surface operations at an airport. GBAS will include multiple spatially separated Global Positioning System (GPS) antennas at each Ground Facility (GF). The primary reasons for the use of multiple reference receivers and antennas at the GF are to provide a means for detection and isolation of a failed receiver and also to allow for a net reduction in ranging error by averaging measurements for a given satellite. However, a generally unrecognized benefit of antenna separation is that differential carrier phase measurements across the antenna baselines can be used to detect and isolate certain signal-in-space (SIS) failures and anomalies that are hazardous to GBAS.

Large ionospheric gradients caused by ionospheric storms are one type of anomaly that has been studied extensively in GBAS [1] and [2]. Existing monitors at the GF exploit the divergence of GPS code and carrier phase observed over time for each satellite to detect these gradients. This approach requires a time history of the measurements and cannot detect gradients present at satellite acquisition. In this case, it is necessary for ground-based fault detection to rely directly on instantaneous GF measurements. In [3], we developed a ground based monitor that uses double difference carrier phase measurements for immediate detection of ionospheric faults. However, this monitor is only capable of detecting gradients in one direction. For precision landing, this implies that the

antennas must be sited parallel to the runway. Such stringent siting requirements can become very costly when trying to service an airport with multi-directional runways. Furthermore, it may not always be possible to align antennas to a runway due to siting limitations.

In this paper, we first generalize the method in [3] to detect ionospheric gradients in any direction using measurements from multiple baselines. A major difficulty with this approach (termed *monitoring algorithm 1*) is the fact that test statistics generated for two baselines sharing a common antenna will be correlated. In this case, it can be extremely complicated to simultaneously set two (or more) thresholds to achieve a specified total probability of false alarm (P_{fa}) and ensure a required probability of missed detection (P_{md}) for a given gradient. In response, an approximate allocation of the P_{md} and P_{fa} is employed that guarantees a conservative assessment of monitor performance.

In order to address the correlation difficulties encountered in monitoring algorithm 1, an alternative approach (termed *monitoring algorithm 2*) is then pursued. This method estimates the gradient vector using double difference carrier phase measurements corrected for the known baseline vector and rounded cycle ambiguities. This allows the measurement error correlation to be properly handled in the measurement noise covariance matrix. The estimated gradient is then used to form a test statistic that is compared to a threshold set according to the continuity requirement. Even though this monitor properly accounts for measurement error correlation, we show that it actually provides worse detection performance than monitoring algorithm 1 due to the nonlinear process of rounding the cycle ambiguities.

A very important ramification of using double difference carrier phase measurements is that the range of detectable ionospheric gradients is highly dependent on the baseline selection in a given reference antenna configuration—that is, how receivers pairs are selected for measurement differencing within a given spatial configuration. Unfortunately, there is no general method for baseline selection that will yield the best detection performance aside from exhaustively evaluating every possibility. In response, another approach is introduced that uses a null space transformation of the between-satellite single difference carrier phase measurement. A major benefit of using the null space transformation is that the detection

performance is always consistent without the need for baseline selection.

II. MONITORING ALGORITHM 1

In [3], a monitor utilizing differential carrier phase measurements across multiple reference stations was introduced to instantaneously detect ionospheric gradients. Here, the monitor is expanded to detect 2-D ionospheric gradient vectors. The simplified double difference carrier phase measurement model between a faulted satellite and a fault-free satellite is given by

$$\Delta^2\phi = \Delta\mathbf{e}^T\mathbf{b} + \lambda\Delta^2n + \Delta I + \Delta^2v \quad (1)$$

where

- $\Delta^2\phi$: double difference carrier phase measurement
- $\Delta\mathbf{e}$: differential user-satellite line of sight unit vector
- \mathbf{b} : baseline vector between two antennas expressed in local NED frame
- λ : carrier wavelength
- Δ^2n : double difference cycle ambiguity
- ΔI : differential ionospheric error between antennas
- Δ^2v : double difference carrier phase measurement noise

It is important to note that the measurement model in equation (1) applies to a single baseline and one satellite pair. Based on experimental analysis of data collected by the Federal Aviation Administration (FAA), it is shown in [3] that the cumulative probability distribution of Δ^2v can be overbounded by a zero-mean Gaussian distribution with variance $\sigma_{\Delta^2\phi}^2 = 36 \text{ mm}^2$. The ionospheric anomaly ΔI is described by the following model [4]

$$\Delta I = \tilde{\mathbf{b}}^T\boldsymbol{\alpha} \quad (2)$$

where

- $\tilde{\mathbf{b}}$: 2×1 vector composed of north and east components of \mathbf{b}
- $\boldsymbol{\alpha}$: 2×1 ionospheric gradient vector

Since $\Delta\mathbf{e}$ and \mathbf{b} are known, they can be combined with $\Delta^2\phi$ in equation (1) to form the new measurement

$$z \equiv \Delta^2\phi - \Delta\mathbf{e}^T\mathbf{b} = \lambda\Delta^2n + \tilde{\mathbf{b}}^T\boldsymbol{\alpha} + \Delta^2v \quad (3)$$

In order to detect the presence of an ionospheric gradient, we must define a detection test statistic. Conceptually, this requires defining a function of the measurement z that will provide us with information about $\boldsymbol{\alpha}$ when an ionospheric gradient is present. Given the measurement model in equation (3), the first step in this process is to remove the effect of Δ^2n on z . This is most easily accomplished through a rounding process. However, it is important to note that there may be a

portion of $\tilde{\mathbf{b}}^T\boldsymbol{\alpha}$ that is close to an integer multiple of λ , and hence will be removed in the rounding process. Therefore, around each integer, there is an undetectable region. More will be said about this concept later in the paper. Accounting for this fact results in the new form for (3)

$$z = \lambda\Delta^2n + \lambda n_\alpha + \tilde{\mathbf{b}}^T\tilde{\boldsymbol{\alpha}} + \Delta^2v \quad (4)$$

where λn_α is the integer portion of $\tilde{\mathbf{b}}^T\boldsymbol{\alpha}$ and $\tilde{\boldsymbol{\alpha}}$ is the remaining part of $\boldsymbol{\alpha}$ that is detectable.

An estimate of $n = \Delta^2n + n_\alpha$ can then be obtained as follows

$$\hat{n} = \text{round}(z / \lambda) \quad (5)$$

Given that the measurement noise is modeled with a standard deviation of 6 mm, the likelihood of rounding the cycle ambiguities incorrectly is extremely small. Therefore, we will assume that $\hat{n} = n$, which allows equation (3) to be written as

$$z - \lambda\hat{n} = \tilde{\mathbf{b}}^T\tilde{\boldsymbol{\alpha}} + \Delta^2v \quad (6)$$

Inserting equation (5) into equation (6) yields

$$z - \lambda \times \text{round}(z / \lambda) = \tilde{\mathbf{b}}^T\tilde{\boldsymbol{\alpha}} + \Delta^2v \quad (7)$$

Therefore, the test statistic is defined as

$$s \equiv z - \lambda \times \text{round}(z / \lambda) \quad (8)$$

Notice from equation (7) that under fault-free conditions ($\boldsymbol{\alpha} = 0$), the test statistic is normally distributed with zero-mean and variance $\sigma_{\Delta^2\phi}^2$.

$$s_{ff} \sim N(0, \sigma_{\Delta^2\phi}^2)$$

where “*ff*” stands for fault-free.

In order to detect ionospheric gradients in multiple directions, test statistics need to be formed from multiple, nonparallel baselines in this monitor. Using separate antennas for each baseline will result in an expensive system. Therefore, it is beneficial to share antennas among the baselines. However, this sharing introduces correlation between test statistics, making it especially difficult to compute the probability of false alarm (P_{fa}) and probability of missed detection (P_{md}). One way to circumvent this problem is to allocate P_{fa} and P_{md} across the baselines such that the true false alarm and missed detection probabilities are always smaller than the specified requirement.

Assuming that we have $m+1$ antennas, we can form m baselines. Then the probability of false alarm and probability of missed detection are defined as

$$\bar{P}_{fa} = P(s_1 > T \cup \dots \cup s_m > T | ff)$$

$$\bar{P}_{md} = P(s_1 < T \cap \dots \cap s_m < T | f)$$

where “ f ” in the second equation stands for the fault event (ionospheric gradient). From elementary probability theory we know that

$$\bar{P}_{fa} \leq P(s_1 > T | ff) + \dots + P(s_m > T | ff)$$

$$\bar{P}_{md} \leq P(s_1 < T | f) + \dots + P(s_m < T | f)$$

Therefore, if we allocate P_{fa} and P_{md} across the baselines such that

$$\sum_{i=1}^m P(s_i > T | ff) = P_{fa} \quad (9)$$

$$\sum_{i=1}^m P(s_i < T | f) = P_{md} \quad (10)$$

then we are guaranteed that monitoring algorithm 1 will always meet the false alarm and missed detection probability requirements.

For a given false alarm requirement P_{fa} and probability of missed detection P_{md} , the minimum detectable error (MDE) was defined in [3] to be

$$MDE = (k_{fa} + k_{md}) \sigma_{\Delta\phi} \quad (11)$$

where the multipliers k_{fa} and k_{md} are derived from the normal cumulative distribution function.

$$k_{fa} = -\sqrt{2} \operatorname{erf}^{-1}(P_{fa} - 1) \quad (12)$$

$$k_{md} = -\sqrt{2} \operatorname{erf}^{-1}(2P_{md} - 1) \quad (13)$$

For quantitative analysis, we use the example requirements from [3]. Based on an availability requirement of 99.9%, P_{fa} is set equal to 10^{-4} . (Recall that the monitor is targeted toward satellites at acquisition so false alarm probability is related to availability and not continuity.) In addition, assuming a 10^{-4} as a prior probability of an ionospheric front occurring, and an integrity risk allocation of 10^{-8} for the threat, P_{md} is set equal to 10^{-4} . These values correspond to multipliers of $k_{fa} = 3.9$ and $k_{md} = 3.7$, and will be used in all quantitative analysis presented in this work.

As noted earlier, portions of the ionospheric gradient will be removed during the rounding process shown in equation (5). Therefore, if $\tilde{\mathbf{b}}^T \boldsymbol{\alpha}$ is close to an integer multiple of λ , the rounding process of equation (5) will remove most of its effect

on the measurement and it will not be detected. This leads to the following undetectable regions for $\boldsymbol{\alpha}$

$$\tilde{n}\lambda - (k_{fa} + k_{md})\sigma_{\Delta\phi} < \tilde{\mathbf{b}}_i^T \boldsymbol{\alpha} < \tilde{n}\lambda + (k_{fa} + k_{md})\sigma_{\Delta\phi} \quad (14)$$

$$i = 1, \dots, m$$

where \tilde{n} is any integer (not to be confused with n) and $\tilde{\mathbf{b}}_i$ is a 2×1 vector composed of the north and east components of the i^{th} baseline vector.

As an example, consider a situation in which four antennas are sited in a square configuration with side length equal to 150m. For this configuration, we have several baseline choices. One possibility is to form three baselines that share a common antenna as shown in Figure 1.a. Another possibility is to consider two sets of parallel baselines as shown in Figure 1.b. In this second case, east and north test statistics can then be formed by averaging the test statistics from the two pairs of baselines. This averaging process effectively reduces the measurement noise variance by a factor of two.

For a given satellite pair, we can vary \tilde{n} in equation (14) to obtain a map of the undetectable region for these two baseline configurations, which are shown in pink in Figure 1. It is clear that choosing two sets of parallel baselines allows larger ionospheric gradients (in a norm sense) to be detected than the configuration with three baselines. This can be seen by considering gradients purely in the east direction. Figure 1.a will detect east gradients up to approximately 950 mm/km while Figure 1.b will detect east gradients up to approximately 1050 mm/km.

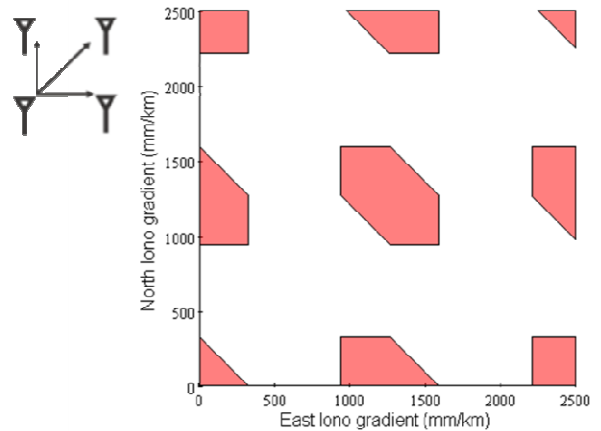


Figure 1.a: Detection performance of monitoring algorithm 1

- baseline selection 1

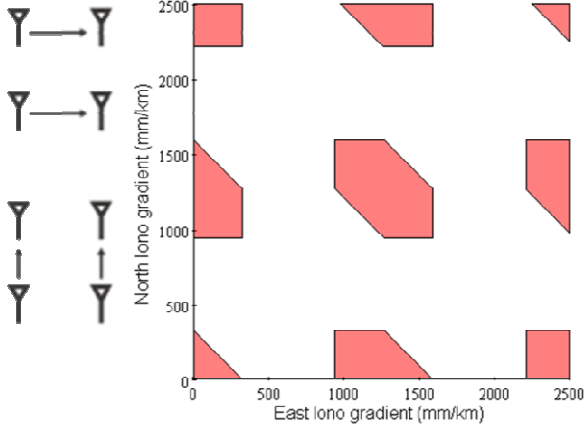


Figure 1.b: Detection performance of monitoring algorithm 1
- baseline selection 2

It is obvious from these results that detection performance is dependent on how the baselines are selected. This is due to the fact that the level of conservatism in the P_{md} and P_{fa} allocation to account for measurement error correlation will vary with how baselines are chosen. Therefore, in order to determine the baseline configuration that yields the best detection performance, we must examine every possible configuration. Clearly, as the number of antennas increases, this process will become computationally cumbersome. Furthermore, it is not evident how to use the method to optimize antenna-siting configurations to maximize detection performance. One potential avenue to eliminate the baseline selection dependency is to rigorously account for measurement error correlation, which leads us to monitoring algorithm 2.

III. MONITORING ALGORITHM 2

Measurement error correlation is encountered frequently in GPS estimation problems—for example, relative position estimation using double difference carrier phase measurements. Because estimators are typically linear, the correlation can be handled in a precise manner. Therefore, our second detection algorithm will use an estimation approach to detect ionospheric gradients so that error correlation among baselines can be accounted for in a rigorous fashion.

Inserting the measurement model from equation (3) into the left hand side of equation (7) results in

$$\begin{aligned}
& z - \lambda \times \text{round}(z/\lambda) \\
&= \lambda \Delta^2 n + \tilde{\mathbf{b}}^T \mathbf{a} + \Delta^2 \mathbf{v} - \lambda \times \text{round} \left[\left(\lambda \Delta^2 n + \tilde{\mathbf{b}}^T \mathbf{a} + \Delta^2 \mathbf{v} \right) / \lambda \right] \\
&= \lambda \Delta^2 n + \tilde{\mathbf{b}}^T \mathbf{a} + \Delta^2 \mathbf{v} - \lambda \times \text{round} \left[\left(\tilde{\mathbf{b}}^T \mathbf{a} + \Delta^2 \mathbf{v} \right) / \lambda + \Delta^2 n \right] \\
&= \tilde{\mathbf{b}}^T \mathbf{a} + \Delta^2 \mathbf{v} - \lambda \times \text{round} \left[\left(\tilde{\mathbf{b}}^T \mathbf{a} + \Delta^2 \mathbf{v} \right) / \lambda \right]
\end{aligned} \tag{15}$$

Stacking all measurements from each baseline for a given satellite pair yields the measurement model

$$\begin{aligned}
\tilde{\mathbf{z}} &= \begin{bmatrix} z_1 - \lambda \times \text{round}(z_1/\lambda) \\ z_2 - \lambda \times \text{round}(z_2/\lambda) \\ \vdots \\ z_m - \lambda \times \text{round}(z_m/\lambda) \end{bmatrix} \\
&= \begin{bmatrix} \tilde{\mathbf{b}}_1^T \\ \tilde{\mathbf{b}}_2^T \\ \vdots \\ \tilde{\mathbf{b}}_m^T \end{bmatrix} \mathbf{a} - \lambda \begin{bmatrix} \text{round} \left(\frac{\tilde{\mathbf{b}}_1^T \mathbf{a} + \Delta^2 v_1}{\lambda} \right) \\ \text{round} \left(\frac{\tilde{\mathbf{b}}_2^T \mathbf{a} + \Delta^2 v_2}{\lambda} \right) \\ \vdots \\ \text{round} \left(\frac{\tilde{\mathbf{b}}_m^T \mathbf{a} + \Delta^2 v_m}{\lambda} \right) \end{bmatrix} + \begin{bmatrix} \Delta^2 v_1 \\ \Delta^2 v_2 \\ \vdots \\ \Delta^2 v_m \end{bmatrix}
\end{aligned} \tag{16}$$

which can be written more succinctly as

$$\tilde{\mathbf{z}} = \mathbf{H}\mathbf{a} - \tilde{\lambda}\tilde{\mathbf{n}} + \Delta^2\mathbf{v} \tag{17}$$

The definitions of \mathbf{H} , $\tilde{\mathbf{n}}$ and $\Delta^2\mathbf{v}$ are obvious by comparing equation (16) to equation (17).

An estimate of the gradient vector is obtained via weighted least squares estimation.

$$\hat{\mathbf{a}} = (\mathbf{H}^T \mathbf{R}^{-1} \mathbf{H})^{-1} \mathbf{H}^T \mathbf{R}^{-1} \tilde{\mathbf{z}} \tag{18}$$

where \mathbf{R} is the covariance matrix of the measurement noise $\Delta^2\mathbf{v}$.

Substituting equation (17) into the right hand side of equation (18) yields

$$\begin{aligned}
\hat{\mathbf{a}} &= (\mathbf{H}^T \mathbf{R}^{-1} \mathbf{H})^{-1} \mathbf{H}^T \mathbf{R}^{-1} (\mathbf{H}\mathbf{a} + \tilde{\mathbf{n}}\lambda + \Delta^2\mathbf{v}) \\
&= \mathbf{a} - (\mathbf{H}^T \mathbf{R}^{-1} \mathbf{H})^{-1} \mathbf{H}^T \mathbf{R}^{-1} \tilde{\mathbf{n}}\lambda + (\mathbf{H}^T \mathbf{R}^{-1} \mathbf{H})^{-1} \mathbf{H}^T \mathbf{R}^{-1} \Delta^2\mathbf{v}
\end{aligned} \tag{19}$$

Defining the estimate error vector $\boldsymbol{\varepsilon} = \hat{\mathbf{a}} - \mathbf{a}$ and noting that $E[\boldsymbol{\varepsilon}] = -(\mathbf{H}^T \mathbf{R}^{-1} \mathbf{H})^{-1} \mathbf{H}^T \mathbf{R}^{-1} \tilde{\mathbf{n}}\lambda$, the estimate error covariance matrix is given by

$$\mathbf{P} = (\mathbf{H}^T \mathbf{R}^{-1} \mathbf{H})^{-1} \tag{20}$$

The test statistic for this monitor is the squared weighted norm of $\hat{\mathbf{a}}$.

$$s = \hat{\mathbf{a}}^T \mathbf{P}^{-1} \hat{\mathbf{a}} \tag{21}$$

which is Chi-square distributed with two degrees of freedom.

The threshold T is computed from the inverse Chi-square distribution based on the P_{fa} requirement. In the presence of an ionospheric fault, the test statistic becomes noncentral Chi-square distributed with a non-centrality parameter λ_{MDE} that defines the monitor's minimum detectable error (MDE). These concepts are illustrated below in Figure 2. Given T and a

requirement on P_{md} , the λ_{MDE} is determined through iteration. Using our example requirements of $P_{fa} = 10^{-4}$ and $P_{md} = 10^{-4}$, the threshold and λ_{MDE} are determined to be 18.42 and 62.82, respectively.

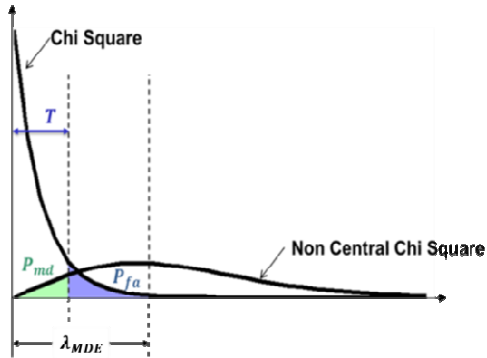


Figure 2: Principles used to define the threshold and MDE

To evaluate this monitor, measurements are simulated according to equation (17) for α vectors ranging from 0 to 2500 mm/km in east and north with antennas placed at the corners of a square with side length equal to 150 m. It is important to note that no measurement noise is added because all of the probabilistic information contained in \tilde{z} has already been accounted for captured in T and MDE. The estimated gradient $\hat{\alpha}$ and test statistic s are then computed from equations (19) and (21). If s is smaller than λ_{MDE} , then that value of α will not be detected with the prescribed P_{md} . Simulation results are shown below in Figure 3.

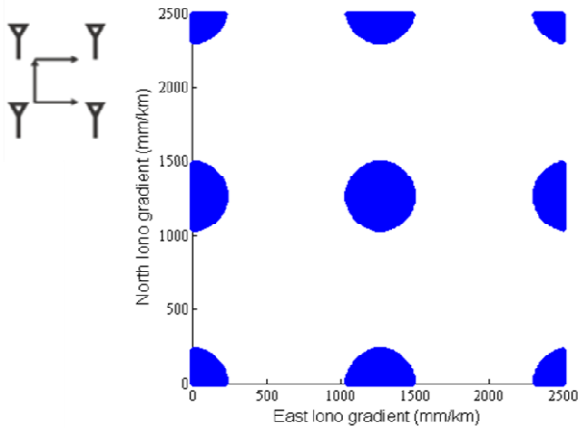


Figure 3.a: Detection performance of monitoring algorithm 2
- baseline selection 1

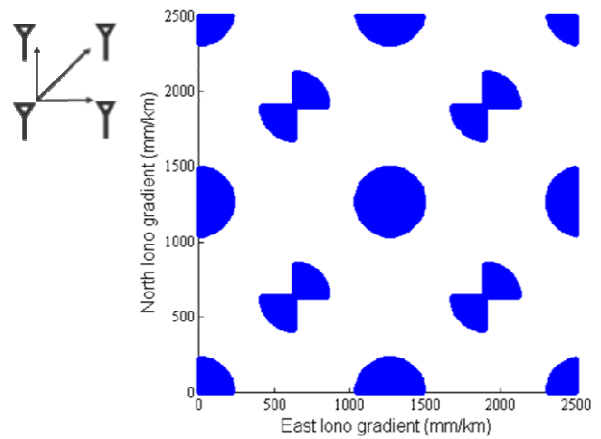


Figure 3.b: Detection performance of monitoring algorithm 2
- baseline selection 2

The blue shaded areas in the Figure 3 indicate that the ionospheric gradient in that region is undetectable. These results clearly show that detection performance is still baseline dependent. However, the reason for this is no longer due to improper treatment of measurement error correlation. Instead, the performance differences are due to the non-linear process of rounding the cycle ambiguities. Therefore, just as in monitoring algorithm 1, we must examine all possible baseline combinations to obtain the best detection performance. To eliminate the baseline selection dependency, a new algorithm is proposed based on null space transformations. It will be the focus of the next section.

IV. NULL SPACE MONITOR

In order to eliminate the baseline configuration dependency in the previous algorithms, a new method is derived based on the null space transformation. To begin, consider the following model for the single difference measurement at antenna 1 between satellites i and j .

$$\begin{aligned} \Delta\phi_1^{ij} &= \mathbf{e}_i^T(\mathbf{x}^i - \mathbf{x}_1) - \mathbf{e}_j^T(\mathbf{x}^j - \mathbf{x}_1) + \Delta I_1^{ij} + \Delta\tau^{ij} + \lambda\Delta n_1^{ij} + \Delta v_1^{ij} \\ &= (\mathbf{e}_i^T \mathbf{x}^i - \mathbf{e}_j^T \mathbf{x}^j - \Delta \mathbf{e}_{ij}^T \mathbf{x}_1 + \Delta\tau^{ij} + \Delta I_1^{ij}) + \lambda\Delta n_1^{ij} + \Delta v_1^{ij} \\ &= \tilde{\rho} + \lambda\Delta n_1^{ij} + \Delta v_1^{ij} \end{aligned} \quad (22)$$

where \mathbf{x}_1 is the position vector of antenna 1, \mathbf{e}_i and \mathbf{e}_j are the line of sight unit vectors for satellites i and j , respectively, ΔI_1^{ij} is the single difference ionospheric error for antenna 1, $\Delta\tau^{ij}$ is the single difference satellite clock bias, Δn_1^{ij} is the single difference cycle ambiguity for antenna 1 and Δv_1^{ij} is the single difference measurement error for antenna 1.

Similarly, the measurement model for antenna 2 is given by

$$\begin{aligned}
\Delta\phi_2^{ij} &= \mathbf{e}_i^T(\mathbf{x}^i - \mathbf{x}_2) - \mathbf{e}_j^T(\mathbf{x}^j - \mathbf{x}_2) + \Delta I_2^{ij} + \Delta\tau^{ij} + \lambda\Delta n_2^{ij} + \Delta v_2^{ij} \\
&= \mathbf{e}_i^T \mathbf{x}^i - \mathbf{e}_j^T \mathbf{x}^j - \Delta \mathbf{e}_{ij}^T \mathbf{x}_1 + \Delta \mathbf{e}_{ij}^T \mathbf{x}_1 - \Delta \mathbf{e}_{ij}^T \mathbf{x}_2 + \Delta \tau^{ij} \\
&\quad + \Delta I_1^{ij} - \Delta I_1^{ij} + \Delta I_2^{ij} + \lambda \Delta n_2^{ij} + \Delta v_2^{ij} \\
&= \tilde{\rho} + \Delta \mathbf{e}_{ij}^T \mathbf{b}_{12} + \tilde{\mathbf{b}}_{12}^T \boldsymbol{\alpha} + \lambda \Delta n_2^{ij} + \Delta v_2^{ij}
\end{aligned} \tag{23}$$

where, in the last step, we have used the following relations

$$\mathbf{b}_{12} = \mathbf{x}_1 - \mathbf{x}_2 \tag{24}$$

$$\tilde{\mathbf{b}}_{12}^T \boldsymbol{\alpha} = -\Delta I_1^{ij} + \Delta I_2^{ij} \tag{25}$$

Since $\Delta \mathbf{e}_{ij}^T \mathbf{b}_{12}$ is a known quantity, it can be moved to the left hand side of equation (23).

$$\Delta\phi_2^{ij} - \Delta \mathbf{e}_{ij}^T \mathbf{b}_{12} = \tilde{\rho} + \tilde{\mathbf{b}}_{12}^T \boldsymbol{\alpha} + \lambda \Delta n_2^{ij} + \Delta v_2^{ij} \tag{26}$$

Stacking measurements from all $m+1$ antennas in one vector results in the linear model

$$\begin{aligned}
\mathbf{z} &= \begin{bmatrix} \Delta\phi_1^{ij} \\ \Delta\phi_2^{ij} - \Delta \mathbf{e}_{ij}^T \mathbf{b}_{12} \\ \Delta\phi_3^{ij} - \Delta \mathbf{e}_{ij}^T \mathbf{b}_{13} \\ \vdots \\ \Delta\phi_{m+1}^{ij} - \Delta \mathbf{e}_{ij}^T \mathbf{b}_{1(m+1)} \end{bmatrix} = \tilde{\rho} \begin{bmatrix} 1 \\ 1 \\ 1 \\ \vdots \\ 1 \end{bmatrix} + \begin{bmatrix} 0 \\ \tilde{\mathbf{b}}_{12}^T \\ \tilde{\mathbf{b}}_{13}^T \\ \vdots \\ \tilde{\mathbf{b}}_{1(m+1)}^T \end{bmatrix} \boldsymbol{\alpha} + \lambda \begin{bmatrix} \Delta n_1^{ij} \\ \Delta n_2^{ij} \\ \Delta n_3^{ij} \\ \vdots \\ \Delta n_{m+1}^{ij} \end{bmatrix} + \begin{bmatrix} \Delta v_1^{ij} \\ \Delta v_2^{ij} \\ \Delta v_3^{ij} \\ \vdots \\ \Delta v_{m+1}^{ij} \end{bmatrix} \\
&= \tilde{\rho} \mathbf{1} + \mathbf{B} \boldsymbol{\alpha} + \lambda \mathbf{n} + \mathbf{v}
\end{aligned} \tag{27}$$

where the definitions of $\mathbf{1}$, \mathbf{B} , \mathbf{n} and \mathbf{v} are obvious.

We can eliminate the term $\tilde{\rho}$ by pre-multiplying both sides of equation (27) by the orthonormal left null space of the vector $\mathbf{1}$.

$$\mathbf{z}' = \mathbf{Lz} = \mathbf{L}\mathbf{B}\boldsymbol{\alpha} + \lambda\mathbf{L}\mathbf{n} + \mathbf{v}' \tag{28}$$

Assuming that the elements of the single difference measurement noise vector \mathbf{v} are uncorrelated, the elements of \mathbf{v}' will also be uncorrelated due to the fact that \mathbf{L} is an orthonormal matrix. Notice that under fault-free conditions (i.e. $\boldsymbol{\alpha} = \mathbf{0}$) and in the absence of noise (i.e. $\mathbf{v}' = \mathbf{0}$), the measurement model in equation (28) simplifies to $\mathbf{z}' = \lambda\mathbf{L}\mathbf{n}$. For different values of the integer vector \mathbf{n} , $\lambda\mathbf{L}\mathbf{n}$ will map to a specific point in the z -space, creating a lattice. From this point forward, we will often refer to \mathbf{L} as a lattice generator.

Even though the null space transformation has eliminated $\tilde{\rho}$, it has introduced a new complication that $\mathbf{L}\mathbf{n}$ is no longer an integer vector. Therefore, the rounding scheme used earlier cannot be applied here. However, we can still use the same

rational to define a test statistic as we did in equation (8). That is

$$s = \|\mathbf{z}' - \lambda\mathbf{L}\hat{\mathbf{n}}\|^2 \tag{29}$$

But the estimate of \mathbf{n} is now determined by solving the following minimization problem

$$\hat{\mathbf{n}} = \arg \min \|\mathbf{z}' - \lambda\mathbf{L}\mathbf{n}\|^2 \tag{30}$$

Many approaches exist in the literature [5], [6] and [7] to solve this minimization problem. However, these methods require the lattice generator \mathbf{L} to be full rank (i.e. a one to one mapping). Because our lattice generator is NOT full rank, we must transform equation (30) into an alternative form. To accomplish this, first note that we can write \mathbf{n} in the form

$$\mathbf{n} = \begin{bmatrix} \mathbf{I} & \mathbf{1} \\ \mathbf{0} & \mathbf{1} \end{bmatrix} \mathbf{n}' \tag{31}$$

Pre-multiplying both sides of equation (31) by \mathbf{L} yields

$$\mathbf{L}\mathbf{n} = \mathbf{L} \begin{bmatrix} \mathbf{I} & \mathbf{1} \\ \mathbf{0} & \mathbf{1} \end{bmatrix} \mathbf{n}' \tag{32}$$

But we know that \mathbf{L} is the left null space of the vector of ones (i.e. $\mathbf{L}\mathbf{1} = \mathbf{0}$), which results in

$$\mathbf{L}\mathbf{n} = [\mathbf{L}'' \quad \mathbf{0}] \mathbf{n}' = \mathbf{L}'' \mathbf{n}'' \tag{33}$$

where \mathbf{L}'' holds the first m columns of \mathbf{L} and \mathbf{n}'' holds the first m components of \mathbf{n}' .

With the equivalence relation shown in equation (33), equations (29) and (30) can be written as

$$s = \|\mathbf{z}' - \lambda\mathbf{L}''\hat{\mathbf{n}}''\|^2 \tag{34}$$

$$\hat{\mathbf{n}}'' = \arg \min \|\mathbf{z}' - \lambda\mathbf{L}''\mathbf{n}''\|^2 \tag{35}$$

Now that \mathbf{L}'' is a full rank lattice generator, the sphere decoder method introduced in [8] will be used to solve the optimization problem shown in equation (35). This method finds all lattice points within a given sphere centered at the measurement vector \mathbf{z}' and determines which one is closest to the center. For a given radius d , the algorithm will find integer vectors $\hat{\mathbf{n}}''$ that satisfy the inequality

$$\|\mathbf{z}' - \lambda\mathbf{L}''\hat{\mathbf{n}}''\|^2 \leq d^2 \tag{36}$$

Notice that the left hand side of equation (36) is identical to the test statistic of the null space monitor. This interesting feature suggests that we can use the sphere decoder algorithm to directly detect the presence of an ionospheric gradient.

Specifically, we can use threshold as the radius, d , if we can find any lattice point inside the sphere, it means that the measurement is in the undetectable region of that lattice point, so the monitor does not alarm. If no lattice point is inside the sphere, the monitor should set the alarm.

The details of the sphere decoder algorithm used in this work are provided in the appendix.

V. MOTIVATIONAL EXAMPLE OF THE NULL SPACE MONITOR

After providing a theoretical development of the null space monitor, it is instructive to analyze its performance for the motivational example of one-dimensional gradient detection with two parallel baselines. The measurement model is restated below for convenience.

$$\mathbf{z}' = \mathbf{Lz} = \mathbf{LB}\alpha + \lambda\mathbf{Ln} + \mathbf{v}' \quad (28)$$

As described earlier, in the absence of noise and under fault-free conditions, $\lambda\mathbf{Ln}$ will create a point lattice in the measurement space. With the inclusion of noise, we get a circle around each lattice point whose radius is given by the λ_{MDE} . This situation is depicted below in Figure 4.

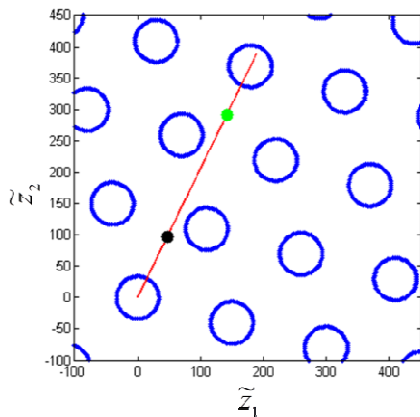


Figure 4: Lattice in measurement domain and ionospheric gradient for selected baselines

Now, in the presence of a fault, the term $\mathbf{LB}\alpha$ defines a line in the measurement space. This is shown as the red line in Figure (4) for baselines with lengths of 100m and 150m. The value of α determines the displacement from the origin. For example, the black and green dots in the Figure 4 correspond to gradient values of $\alpha=1000$ mm/km and $\alpha = 3000$ mm/km, respectively. The ionospheric gradients inside any circle are undetectable by this monitor.

The threshold and MDE is computed in the similar way as in the estimation method. That is, MDE is determined from the non-centrality parameter for a noncentral Chi-squared distribution with m degrees of freedom. Recall from the discussion of Figure 4 that the line is described by the equation $\tilde{\mathbf{z}} = \mathbf{LB}\alpha$. Therefore we can use the pseudo-inverse matrix to map undetectable ionospheric gradients from the measurement domain back to the gradient domain.

$$\alpha = ((\mathbf{LB})^T \mathbf{LB})^{-1} (\mathbf{LB})^T \tilde{\mathbf{z}} \quad (37)$$

Consider an example where one baseline is fixed at 100 m while the other baseline is allowed to vary from 0 to 300 m. Figure 5.a shows the performance of monitoring algorithm 1 while Figure 5.b shows the performance of the null space monitor. In both figures, the blue shaded area corresponds to undetectable regions while the white space corresponds to detectable ionospheric gradients. It is clear by comparing these two Figures that the null space monitor is capable of detecting more gradients than monitoring algorithm 1.

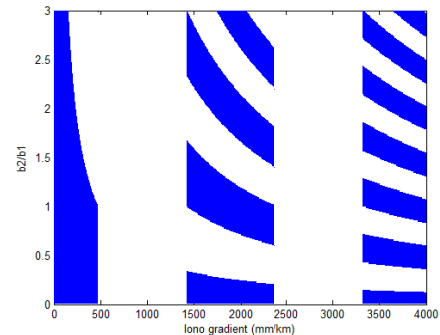


Figure 5.a: 1-D Detection performance of monitoring algorithm 1



Figure 5.b: 1-D Detection performance of null space monitor

The null space monitor can also be used to detect two-dimensional gradients. However the situation becomes more complicated. For one-dimensional gradient detection, it was shown in Figure 4 that the problem could be presented in terms of a lattice of circles intersected by a line. For two-dimensional detection with four antennas, the analogous situation is a lattice of spheres intersected by a plane.

Using the same square antenna configuration that was considered in monitoring algorithms 1 and 2, the null space monitor yields performance as shown in Figure 6.

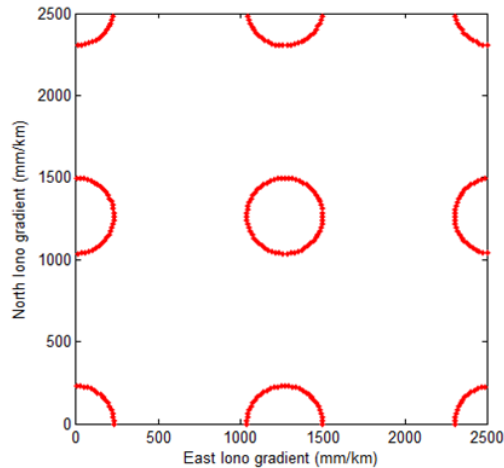


Figure 6: Detection performance of null space monitor

Ionospheric gradients outside the circles can be detected while those inside the circles cannot be detected. These results can be superposed with the results from monitoring algorithms 1 and 2, as shown in Figure 7.

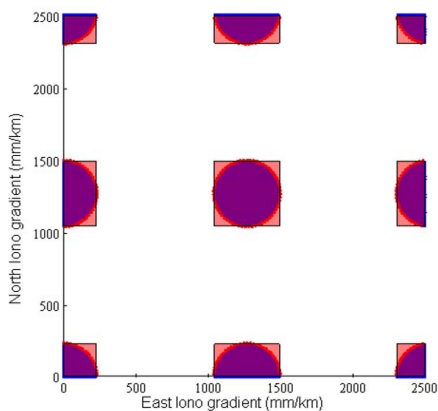


Figure 7: Comparison of three algorithms

The blue area indicates the undetectable region for monitoring algorithm 2; the pink polygon is the undetectable region of monitoring algorithm 1 and inside the red circle is the undetectable region of null space monitor. For this particular baseline configuration, the performance of the null space monitor is equivalent to that of monitoring algorithm 2. This is a special case, and this conclusion does not hold in general. For example, consider the antenna configuration and baseline selection shown in Figure 8. In this case, the null space monitor's detection performance is far superior to that of monitoring algorithms 1 and 2.

Investigation into the benefits of the null space monitor has only just begun. Future work will focus on providing a methodology to determine the antenna configuration that yields the maximum detectable ionospheric gradient subject to requirements on the probability of false alarm and minimum detectable error. The potential for the method to detect GPS orbit ephemeris faults will also be investigated.

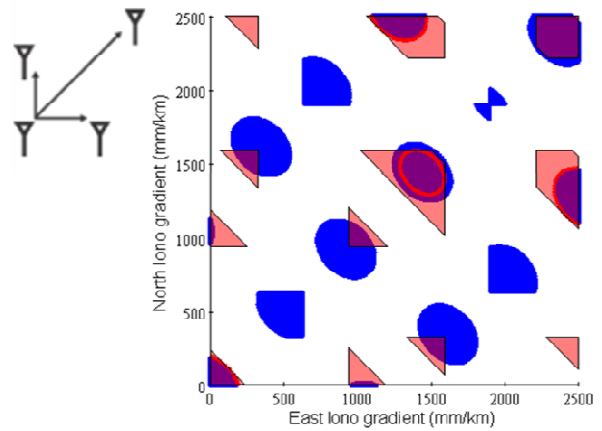


Figure 8: Comparison of the three algorithms in another antenna configuration

VI. CONCLUSION

In this work, three monitoring algorithms were proposed for the detection of ionospheric gradients using multiple reference station antennas. Two of these monitors were designed using traditional methods from detection and estimation theory, and their performance was shown to be dependent on the specific baseline selection between the antennas. This adverse effect implies that all possible baseline configurations must be exhaustively examined to determine which one yields the maximum detectable ionospheric gradient. As the number of reference antennas increases, these approaches are computationally difficult, and they are infeasible when optimization of antenna placement is considered. In response, a third monitor was proposed based on the null space transformation of between-satellite single difference measurements. The underlying detection algorithm was derived in terms of a lattice search, and it was shown that the performance of this monitor is independent of baseline selection, and has generally better detection performance. The null space monitor is currently the most efficient algorithm for ionospheric gradient detection in Ground Based Augmentation Systems.

APPENDIX

To find the minimizer integers for our problem, the first step is to perform a QR decomposition on the lattice generator, \mathbf{L}'' .

$$\mathbf{L}''_{m \times m} = \mathbf{QR} \quad (37)$$

\mathbf{R} : $m \times m$ upper triangular matrix with positive diagonal elements

\mathbf{Q} : $m \times m$ unitary matrix

If we express equation (34) as a quadratic form and use the properties of a unitary matrix, we can write the inequality in the form

$$\|\mathbf{z}'' - \lambda \mathbf{R} \hat{\mathbf{n}}''\|^2 \leq d^2 \quad (38)$$

where $\mathbf{z}'' = \mathbf{Q}^T \mathbf{z}'$.

Because \mathbf{R} is an upper triangular matrix, equation (38) is equal to:

$$\sum_{j=i}^m \left(z_j'' - \lambda \sum_{l=j}^m r_{j,l} \hat{n}_l'' \right)^2 \leq d^2, \quad i=1, \dots, m \quad (39)$$

where $r_{j,l}$ is the (j, l) element of \mathbf{R} .

Starting from the last element (when $i = m$) yields

$$\left(z_m'' - \lambda r_{m,m} \hat{n}_m'' \right)^2 \leq d^2 \quad (40)$$

Because the diagonal elements of \mathbf{R} are positive, upper and lower bounds on the permissible values of \hat{n}_m'' are given by

$$\hat{n}_{m,\max}'' = \left\lfloor \frac{1}{\lambda r_{m,m}} (z_m'' + d) \right\rfloor, \quad \hat{n}_{m,\min}'' = \left\lceil \frac{1}{\lambda r_{m,m}} (z_m'' - d) \right\rceil \quad (41)$$

where

$\lfloor \cdot \rfloor$: rounding to the nearest integer towards plus infinity

$\lceil \cdot \rceil$: rounding to the nearest integer towards minus infinity

The integer candidates for \hat{n}_m'' must then be in the range $[\hat{n}_{m,\min}'', \hat{n}_{m,\max}'']$.

In general, for the i^{th} element we have

$$\sum_{j=i}^m \left(z_j'' - \lambda \sum_{l=j}^m r_{j,l} \hat{n}_l'' \right)^2 \leq d^2 \quad (42)$$

Making the definition

$$\Lambda_{i+1} = \sum_{j=i+1}^m \left(z_j'' - \lambda \sum_{l=j}^m r_{j,l} \hat{n}_l'' \right)^2 \quad (43)$$

equation (42) can be also be written as

$$\left(z_i'' - \lambda \sum_{l=i}^m r_{i,l} \hat{n}_l'' \right)^2 + \Lambda_{i+1} \leq d^2 \quad (44)$$

Separating the sum on the right hand side of equation (44) results in

$$\left(z_i'' - \lambda r_{i,i} \hat{n}_i'' - \lambda \sum_{l=i+1}^m r_{i,l} \hat{n}_l'' \right)^2 + \Lambda_{i+1} \leq d^2 \quad (45)$$

which yields the following bounds on the possible integer values of \hat{n}_i .

$$\begin{aligned} \hat{n}_{i,\max} &= \left\lfloor \frac{1}{\lambda r_{i,i}} \left(z_i'' - \lambda \sum_{l=i+1}^m r_{i,l} \hat{n}_l'' + (d^2 - \Lambda_{i+1})^{1/2} \right) \right\rfloor, \\ \hat{n}_{i,\min} &= \left\lceil \frac{1}{\lambda r_{i,i}} \left(z_i'' - \lambda \sum_{l=i+1}^m r_{i,l} \hat{n}_l'' - (d^2 - \Lambda_{i+1})^{1/2} \right) \right\rceil \end{aligned} \quad (46)$$

This process is completed for $j = m, m-1, m-2, \dots, 1$, and provides a feasible region for the cycle ambiguities.

REFERENCES

- [1] Pullen, S., Y. S. Park, and P. Enge, "Impact and mitigation of ionospheric anomalies on ground-based augmentation of GNSS," Radio Science, Vol. 44, RS0A21, doi:10.1029/2008RS004084, 2009.
- [2] Gratton, L., Chan, F., Pervan, B., "Algorithms for Airborne Ionospheric Front Detection in LAAS Using Carrier Phase and INS Measurements," Proceedings of the 2005 National Technical Meeting of The Institute of Navigation, San Diego, CA, January 2005, pp. 131-139.
- [3] Khanafseh, Samer M. et al. "Carrier Phase Ionospheric Gradient Ground Monitor for GBAS with Experimental Validation." Proceedings of the 23rd International Technical Meeting of the Satellite Division of the Institute of Navigation (ION GNSS-2010), Portland, OR, September 21-24, 2010.
- [4] Ming Luo "LAAS Study of Slow-Moving Ionosphere Anomalies and Their Potential Impacts. " ION GNSS 18th International Technical Meeting of the Satellite Division, 13-16 September 2005, Long Beach, CA
- [5] R. Kannan, "Improved algorithms for integer programming and related lattice problems," in Proc. ACM Symp. Theory of Computing, Boston, MA, Apr. 1983, pp. 193-206.
- [6] E.Agrell, "Closest Point Search in Lattices," IEEE Transactions on Information Theory, VOL.48, No.8, Aug.2002.
- [7] L. Babai, "On Lovász' lattice reduction and the nearest lattice point problem," Combinatorica, vol. 6, no. 1, pp. 1-13, 1986.
- [8] Mohamed Oussama Damen. "On Maximum-Likelihood Detection and the Search for the Closest Lattice Point." IEEE Transactions on Information Theory, VOL. 49, NO. 10, Oct. 2003.